Smart Mater. Struct. **22** (2013) 105007 (12pp) doi:10.1088/0964-1726/22/10/105007

A multi-feature integration method for fatigue crack detection and crack length estimation in riveted lap joints using Lamb waves

Jingjing He[1], Xuefei Guan[1], Tishun Peng[1], Yongming Liu[1], Abhinav Saxena[2], Jose Celaya[2] and Kai Goebel[3]

[1] School for Engineering of Matter, Transport, and Energy, Arizona State University, Tempe, AZ 85281, USA
[2] SGT, NASA Ames Research Center, Moffett Field, CA 94035, USA
[3] NASA Ames Research Center, Moffett Field, CA 94035, USA

E-mail: yongming.liu@asu.edu

Received 14 February 2013, in final form 7 July 2013
Published 4 September 2013
Online at stacks.iop.org/SMS/22/105007

Abstract
This paper presents an experimental study of damage detection and quantification in riveted lap joints. Embedded lead zirconate titanate piezoelectric (PZT) ceramic wafer-type sensors are employed to perform *in situ* non-destructive evaluation (NDE) during fatigue cyclical loading. PZT wafers are used to monitor the wave reflection from the boundaries of the fatigue crack at the edge of bolt joints. The group velocity of the guided wave is calculated to select a proper time window in which the received signal contains the damage information. It is found that the fatigue crack lengths are correlated with three main features of the signal, i.e., correlation coefficient, amplitude change, and phase change. It was also observed that a single feature cannot be used to quantify the damage among different specimens since a considerable variability was observed in the response from different specimens. A multi-feature integration method based on a second-order multivariate regression analysis is proposed for the prediction of fatigue crack lengths using sensor measurements. The model parameters are obtained using training datasets from five specimens. The effectiveness of the proposed methodology is demonstrated using several lap joint specimens from different manufactures and under different loading conditions.

(Some figures may appear in colour only in the online journal)

1. Introduction

Guided ultrasonic waves have shown great potential in non-destructive evaluations (NDE) and structural health monitoring (SHM) systems. Use of guided ultrasonic waves allows for the inspection of a large area in a short time scale for both isotropic and anisotropic materials [1, 2]. Commercially available low-cost sensors enable the use of guided Lamb wave inspection technique in many disciplines for health monitoring. Lamb waves are a form of elastic perturbation, which can be used to interrogate the integrity of a target system [3]. Their dispersion characteristics in a plate have been studied by the Rayleigh–Lamb equation [4, 5]. Lamb wave propagation and speed are sensitive to plate thickness and are expected to change due to the existence of structural defects [6–8]. A large number of publications have reported on damage identification using Lamb waves [2, 9–16]. Techniques for damage identification using Lamb waves can be classified into two categories [15]: the pulse–echo method and the pitch–catch method. In the pulse–echo method, a narrow bandwidth pulse excites the system and a sensor is used to sense echoes of the pulse

generated by material discontinuities. In the pitch–catch method, a pulse signal is sent across the specimen to interrogate the integrity of the specimen. At the same time, a sensor is placed at the other end of the specimen to receive the signal. In both methods, damage-sensitive features might be obtained from the measurement data using signal processing algorithms. Characteristics such as the attenuation and phase shift can be used to extract the damage information [15] of the system being inspected.

In recent years, the generation of Lamb waves with piezoelectric (PZT) ceramic wafers has drawn intensive attention from the SHM community [17–23]. PZT wafers are inexpensive, non-intrusive, and can be permanently attached to a structure. Many studies have been reported on practical applications of PZT wafers to specific target systems, for example, plates [14, 17, 24–26] and beam structures [1, 27]. The Lamb wave propagation results in splitting of the wave energy into several modes, which are analyzed to look for internal features of the composite material. The characteristics of three transmission modes (S_0, A_0 and A_1 modes) propagating in adhesively bonded lap joints were investigated in [28], where finite element analysis was used to calculate transmission coefficients for the three modes. The study provided a basis for mode selection for the Lamb wave NDE of the bond region in a lap joint [28]. An analytical and experimental study of the PZT damage identification performance was reported in [17], where theoretical developments were studied in order to clarify the mechanism through which PZT sensors can be manipulated to excite ideal modes, and experimental damage detection was performed in aircraft panels adjacent to rivet heads. The pulse–echo method was used to detect a crack (12.7 mm) that was artificially inserted into the panel. Detection of the crack in a lap joint using raw pulse–echo measurement data might be difficult because echoes from the rivet and from the crack are superimposed. This difficulty can be reduced by subtracting a baseline signal recorded on the undamaged structure from the signal recorded on the damage structure [17]. Signal processing techniques, such as Hilbert transforms and time-frequency analysis have been proposed to interpret the signal collected from PZT sensors in riveted aluminum strap joints [29]. Grondel *et al* [29] also used an acoustic emission system to make a comparison with the results obtained from Lamb wave analysis. The result showed that the Lamb wave technique has the capability of monitoring crack initiation and locating the crack damage. Numerical simulations for damage detection in 2D and 3D lap joints using the Lamb wave method is proposed in [30], where propagation of the S_0 mode and its interaction with discontinuities were studied using the finite difference method and the finite element method. In [31] a support vector machines (SVM)-based classifier was used to detect the crack damage on single lap bolted joints caused by torque loss. 100% torque case, 50% torque case and 0% torque case were studied. The result indicated that the method can detect completely loose bolts but certain changes in torque can introduce non-unique solutions under certain conditions. In [32] Lindgren *et al* reported the effect of varying the boundary conditions in a multi-layered metallic structure (consisting of 2–4 total layers) on the propagation of ultrasonic plate waves. The variation of the boundary conditions was simulated by applying various loading on the surface of each layer. The experimental and theoretical work indicated the interface condition between the layers affects the ultrasonic wave propagation. Therefore, changes of the interface condition must be considered when performing damage detection using ultrasonic plate waves for multi-layered structures [32]. In [33] a tomography algorithm was proposed to detect and locate the fatigue crack in an aluminum plate. Amplitude ratio of the S_0 Lamb wave mode and signal difference coefficient were used to size the crack. The results showed that both an amplitude ratio and the signal difference coefficient are sensitive to a fatigue crack emanating from 12.7 mm diameter fastener hole [33].

Despite several advancements reported on this topic, there are still several challenges in Lamb wave-based damage detection and quantification. Most studies have so far focused on the simple geometry of plate structures with a hole or a cut to represent the damage. Realistic fatigue cracks initiated from structural components with complex local geometries are rarely investigated. In addition, the subtle variability between different specimens may cause uncertainties for damage detection. For example, different manufacturing and environmental conditions will lead to variability of components/structures even when they are designed to be identical. The uncertainties must be carefully investigated for realistic applications. The study reported here investigates damage detection for naturally initiated fatigue cracks in fuselage lap joint specimens instead of using artificially inserted crack-like defects. Multiple specimens from different manufactures and under different loadings are tested to investigate the variability effect on damage detection. A multi-feature integration method is proposed to quantify the crack size with measurement data.

The paper is organized as follows. First, the experiment design is introduced briefly. Undamaged specimens are used to understand and characterize the Lamb wave generation, and verify the group velocity dispersion curve. Next, fatigue tests are performed on aircraft lap joint specimens. PZT sensors are installed on the specimens, and are used to collect data for the riveted regions. Following this, measured data are processed using band-pass filtering to reduce the effect of measurement noise for damage feature extraction. Three damage features and a multivariate regression model are proposed to correlate the damage features to the actual crack size. Experimental testing data from five specimens are used to estimate model parameters and two additional specimens are used to validate the effectiveness of the model. Finally, conclusions are drawn based on the current investigation.

2. Experiment design

The underlying mechanism for Lamb wave detection is to monitor the changes of the characteristics of the transmitted/deflected waves. The changes of the characteristic are due to discontinuities introduced by material defects such

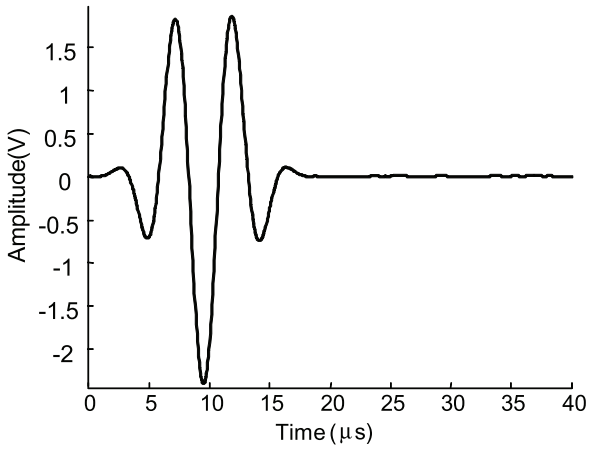

Figure 1. A tone burst signal of 3.5 cycles and 200 kHz central frequency. This signal is used as the excitation signal in this study.

as cracks and voids in the path of wave propagation. The discontinuities can disperse and reflect energy of the original Lamb wave and cause changes in wave characteristics. The changes, in principle, can be detected and used to locate the damage and quantify the severity [34]. Existing literature shows that at lower frequencies, fewer Lamb modes are excited so the response signal is more distinguishable [2, 3, 17]. In addition, the detection of through thickness cracks is much better with the S_0 mode than with the A_0 mode [18]. The tuning of desired modes at certain frequencies can be achieved based on the fact that wavelengths of Lamb wave modes vary with frequency. Giurgiutiu reported that 300 kHz is a proper frequency for the S_0 mode when using a 7 mm diameter PZT sensor attached to a 1 mm-thick aluminum plate [18]. The velocity of the Lamb wave is a function of the product of frequency f and plate thickness d (fd, expressed in MHz mm). Ideally, the S_0 mode is sensitive to small damage and is best exploited at very low value of fd [2, 17, 28–30]. Based on the previous experience, the product of the frequency and plate thickness is chosen to be 0.32 MHz mm. In the vicinity of 0.32 MHz mm, the S_0 wave is highly non-dispersive with a group velocity that is almost constant and the A_0 wave is highly dispersive. The specimens employed in this study have a thickness of 1.6 mm and the central frequency is set to be 200 kHz. A Hamming-windowed sinusoidal tone burst with 3.5 cycles is used as the excitation signal, as shown in figure 1.

2.1. Specimens: material and geometry

The riveted panels are made of 1.6 mm thickness aircraft grade 2024-T3 aluminum sheets and were originally provided by the National Research Council (NRC) Canada [35]. For repeatability, additional coupons were manufactured at NASA Dryden Flight Research Center. All the specimens have the same geometry and were made of the same material. The specimens are three rivet rows by five rivets wide lap joints, consisting of two aluminum panels. The top panel has a countersunk hole and the bottom panel has a straight hole, as shown in figure 3. The detailed geometry of the specimen is shown in figure 2. The yield strength of the material is 360 MPa, the ultimate strength is 490 MPa, and the Young's modulus is 72 000 MPa. Results from existing data indicate

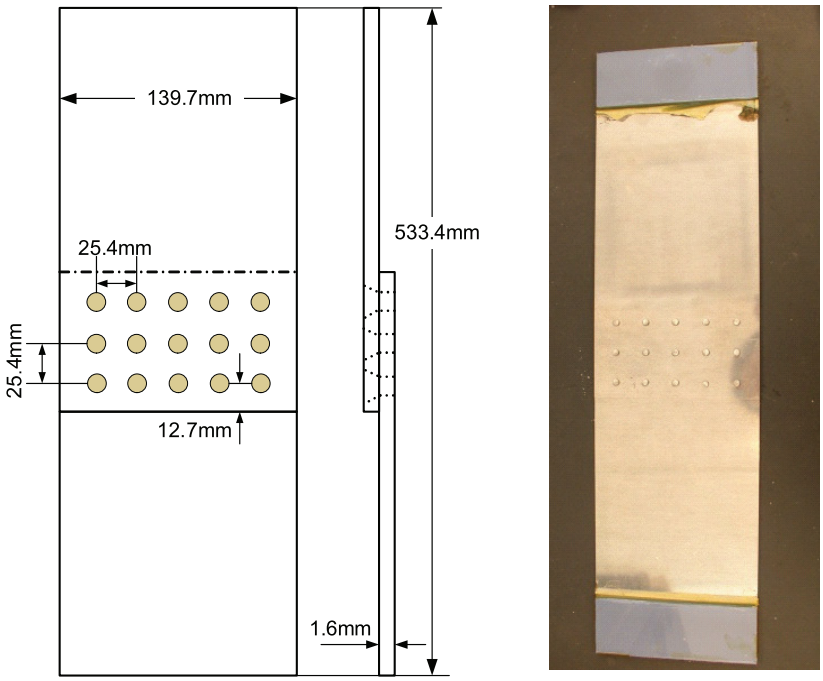

Figure 2. Geometry of the lap joint specimen.

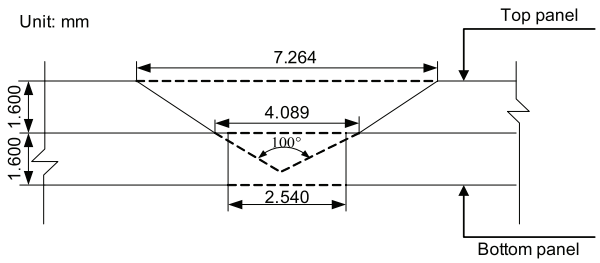

Figure 3. Detailed local geometry of the bolt connection.

that the countersunk hole has a larger stress concentration and the first row of the rivet at the top panel is the most probable location (hot spot) to develop fatigue damage.

2.2. Experimental setup

The overall experimental setup of the structural health monitoring system for riveted lap joint consists of three major parts: sensing and data acquisition system, fatigue crack optical measurement system, and fatigue cycling system. A schematic of the overall procedure is shown in figure 4. Sensing and data acquisition system generates an excitation signal and senses the wave propagating though the specimen including damaged regions. The excitation signal was a 3.5 cycle tone burst generated by a function generator. A multi-channel digital oscilloscope is used to record both the received signal and the excitation signal. PZT (SM412) sensors from Steaming company is used as the actuator to excite guided Lamb waves, as well as the sensor to acquire guided wave signal. The chosen PZT has a dimension of 7 mm diameter $\times$ 0.2 mm thickness, and the resonant frequency is 300 kHz $\pm$ 10 kHz. Regions vulnerable to fatigue damage are monitored by a traveling optical microscope with a CCD camera during the fatigue testing process. Fatigue testing is conducted using a hydraulic MTS machine with 5 Hz cycling frequency and at room temperature. Both constant fatigue loading and variable fatigue loading cases are studied. Figures 5(a) and (b) presents the constant and variable amplitude loading spectra used in this study, respectively. The overall experimental setup is shown in figure 6.

2.3. Group velocity test

The group velocity is estimated to select an appropriate time window during which signal properties may change due to any discontinuity in the fatigue-vulnerable region of the specimen. The group velocity of the generated Lamb wave at a particular frequency can be verified in an undamaged specimen by measuring the time-of-flight (TOF) between two sensors with known separation. As shown in figure 7, the black line represents the guided Lamb wave sent by the actuator at one location and the red line represents the signal received by the receiver at another location. The calculated group velocity of the wave was estimated at 4755.4 m s^{-1}.

2.4. Sensor network design

The sensor network design is critical for damage detection using the Lamb wave. In the pulse–echo configuration, the actuator and receiver are placed on the same side of the potential damage region under interrogation. In the pitch–catch configuration, the actuator and the receiver are placed across the potential damage region. One limitation for the pulse–echo configuration is that it may not be sensitive to damage at a remote location. Comparing with the pitch–catch configuration, the signal in pulse–echo method travels a relatively longer distance and may lose substantial information for damage feature extraction [36]. The first

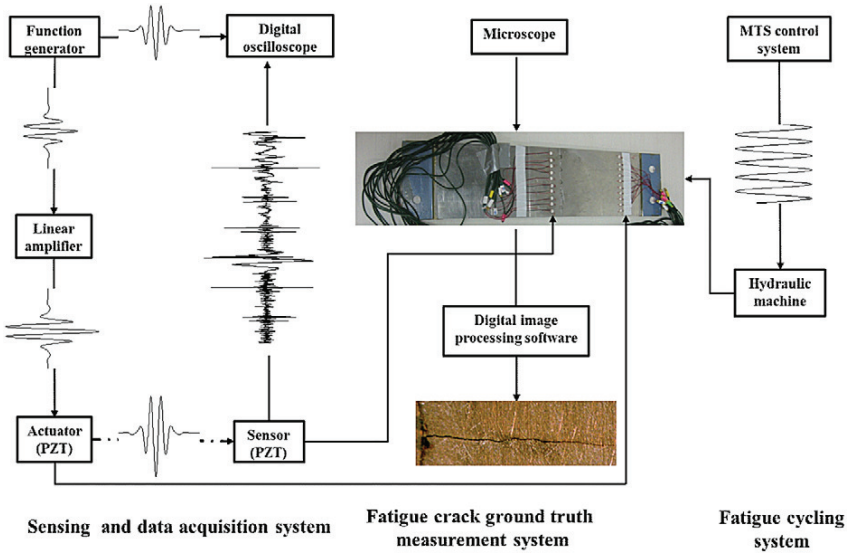

Figure 4. Systematic flowchart for the health monitoring system for riveted lap joints.

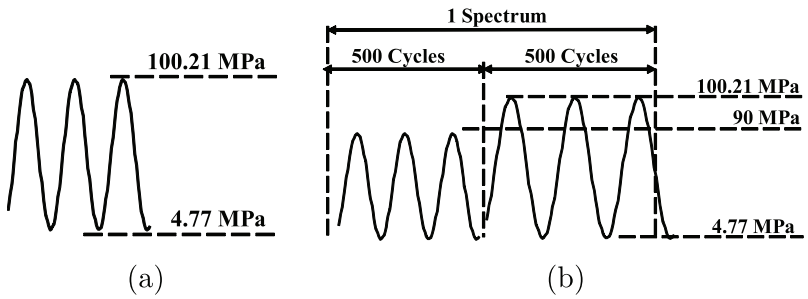

Figure 5. Fatigue loading spectra for riveted lap joints. (a) Constant loading spectra and (b) variable loading spectra.

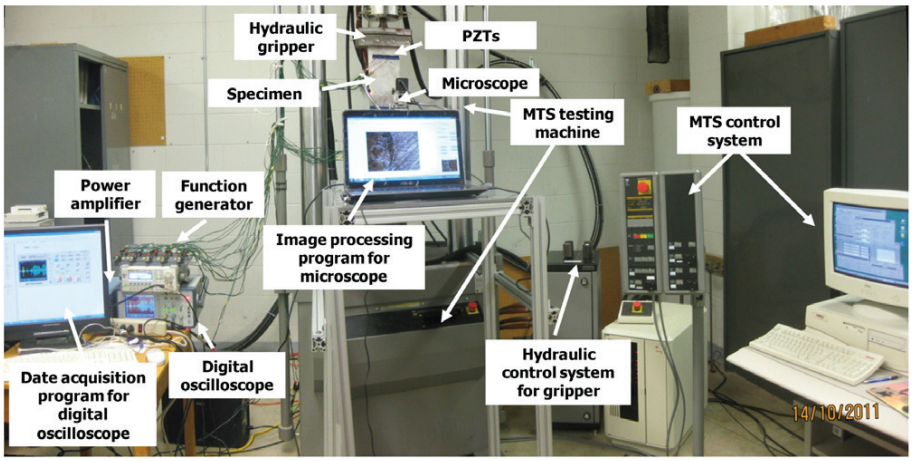

Figure 6. Experimental setup for the riveted lap joint fatigue testing and data acquisition.

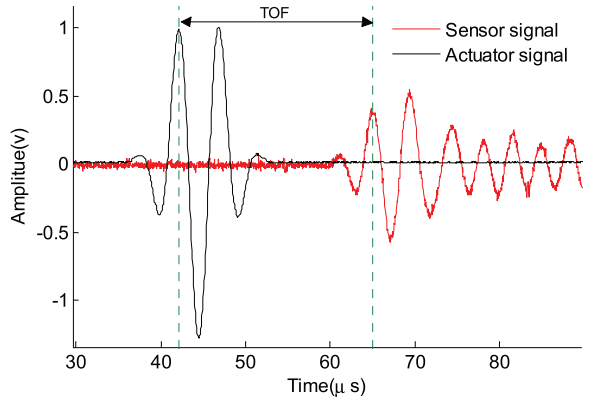

Figure 7. Group velocity test using an actuator (signal in black) and a receiver (signal in red) at known locations.

and third rows are possible locations for crack initiation according to the principle of design. According to the existing experimental data from NRC Canada and our in-house testing, the crack usually initiates at the countersunk hole in the first row. The crack will connect these holes and finally break the specimen. As a result, the countersunk hole in the first row is marked as the target area in this study (see figure 8). It can be seen from the illustration that the target region is close to the boundary where two aluminum panels are connected. For the pulse–echo configuration, the echo from the boundary and the echo from the possible discontinuity introduced by the damage are difficult to be separated due to superposition of the two echoes. Considering that, the pitch–catch configuration is employed in this study. The sensor placement layout is shown in figure 8, where red dots represent actuators and the green dots represent receivers near the target region. For each row of the rivet hole lines (five lines in total), two PZT sensors are placed on each side of the line.

2.5. Time window calculation

With the knowledge of group velocity and physical distance between the target region and the actuator, an appropriate time window is chosen to extract signal features from measured time series. The calculation of the time window is based on equations (1) and (2). T_1 is the starting point chosen from the actuator signal and it represents the beginning of a wave sent from an actuator. T_2 is the time duration for the Lamb wave to travel from an actuator to the target region (see figure 9). In equation (2), T_{start} represents the time point at which the first Lamb wave package arrives at the target area, and T_{end} represents the time point at which the Lamb wave passes through the target region. The time duration between T_{start} and T_{end} is the desired time window during which one Lamb wave package travels through the target region.

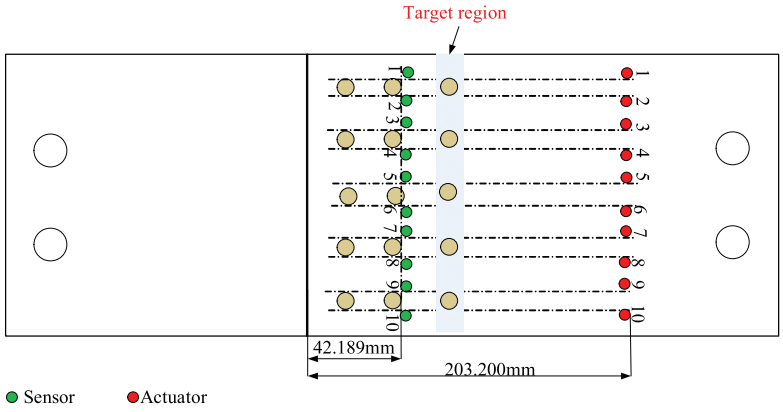

Figure 8. PZT sensor layout for damage detection in riveted lap joints.

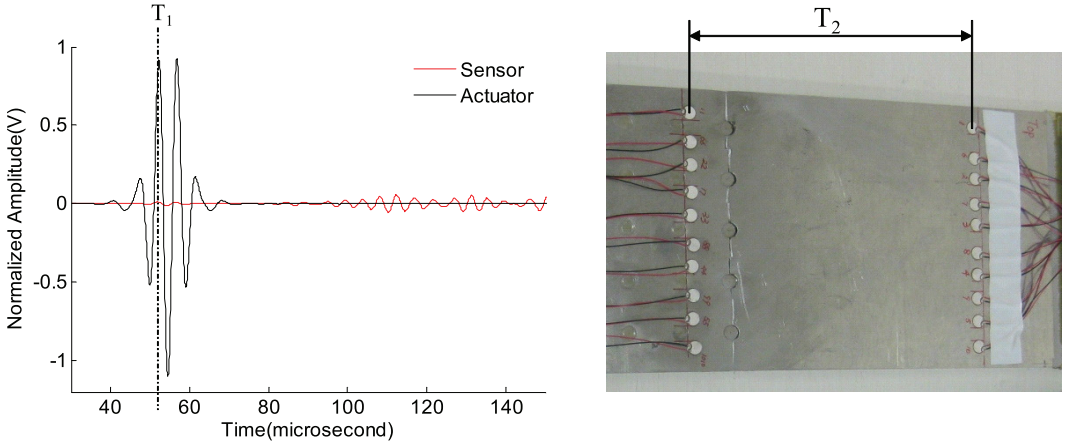

Figure 9. Schematic illustration for the time window calculation.

Characteristics of the measurement data in this time window are expected to change due to any discontinuity introduced by fatigue damage.

$$T_{\text{start}} = T_1 + T_2. \quad (1)$$

$$T_{\text{end}} = T_{\text{start}} + 1/200\,000 \times 3.5. \quad (2)$$

3. Experimental results and the signal processing technique

Seven specimens are used for testing. Fatigue cracks are naturally generated during fatigue testing. Detailed information on fatigue loading spectra and the location of resulting cracks is presented in table 1. Specimens T1–T6 were manufactured at NASA Dryden Flight Research Center and N1 is the specimen manufactured at NRC Canada. Figure 10 shows a plot of the number of load cycles versus the crack length for all the specimens. The crack length measurement obtained using a traveling microscope is considered as the ground truth size of the crack. A significant variability among specimens is observed from figure 10 and table 1.

Table 1. Riveted lap joints fatigue testing summary.

Specimen no.	Fatigue life (cycles)	Crack initiation location	Loading spectrum
T1	70 766	Sensor no. 4	Constant
T2	72 127	Sensor no. 8	Constant
T3	67 401	Sensor no. 6	Constant
T4	100 774	Sensor no. 2	Block loading
T5	75 045	Sensor no. 9	Constant
T6	49 448	Sensor no. 4	Constant
N1	55 031	Sensor no. 8	Constant

At each of the measurement points shown in figure 10, the fatigue testing experiment was paused for data acquisition. Lamb waves were generated by the actuator and the transmitted waves are collected by the sensors. The Lamb wave data acquisition process is repeated twice to eliminate the operation error during each of the pauses. At the mean time, the microscopic imaging is carried out to record the crack size. Fatigue testing is resumed after data acquisition. For demonstration purposes, the raw measurement data for one of the recorded points plotted in figure 10 (specimen T1 indicated by the arrow) are presented in figure 11(a). It can be observed that the two repeated measurements exhibit some

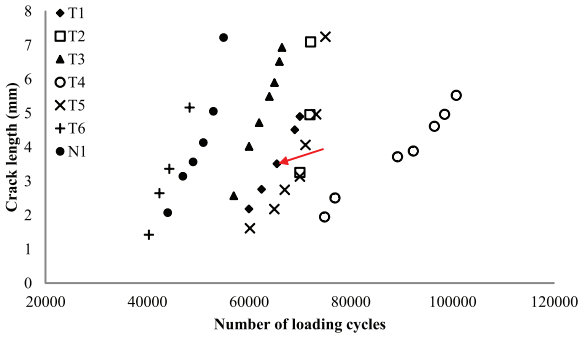

Figure 10. Fatigue testing data.

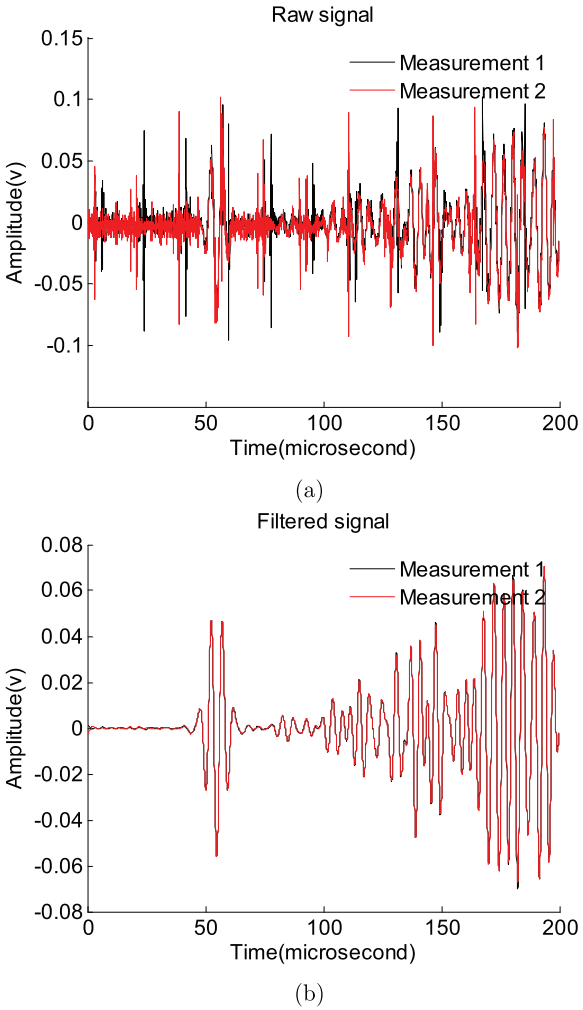

Figure 11. Measurements taken from the same transducer. (a) Raw signals and (b) de-noised signals.

differences due to measurement noise, which can be caused by various sources, such as environmental conditions, specimen boundary conditions, vibration introduced noise, sensitivity of the electronic system and electric fluctuations, etc. In order to extract useful Lamb wave data from the raw data, a band-pass filter is designed and used for data de-noising. The pass-band

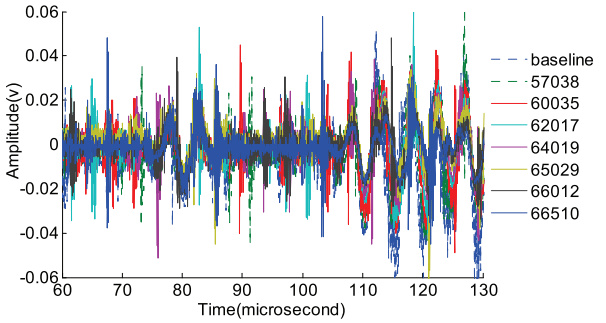

Figure 12. Raw signal data from sensor at different loading cycles for specimen T3.

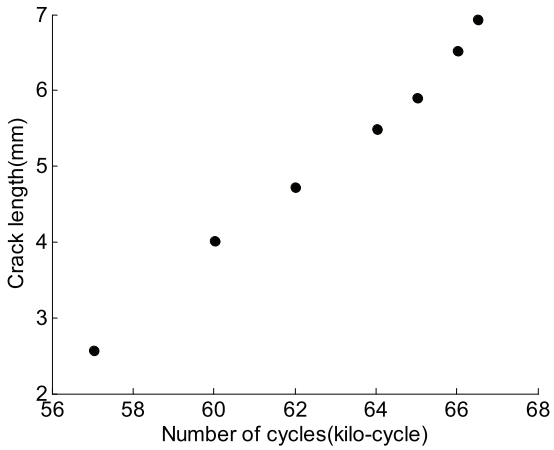

Figure 13. Crack size measurement at different loading cycles for specimen T3.

corner frequency is [100 200] kHz and the stop-band corner frequency is [250 450] kHz. As shown in figure 11(b), the two sets of de-noised data acquired by the same sensor are almost identical (the correlation coefficient between the two sets of data is 0.9997).

In fatigue testing, the baseline signals are collected prior to any fatigue damage in the specimens. The baseline signal is used as a reference for comparison with damage signals for damage feature extraction. Fatigue crack initiation and growth are tracked using microscopic imaging. The crack length measurement results (obtained by image registration technique with microscopic imaging) and the extracted damage features are used to develop a damage model that correlates the crack length and the measurement data. Measurement data for specimen T3 are selected here for demonstration. Figure 12 presents the raw measurement data from the PZT sensors at different crack lengths. Figure 13 presents the fatigue testing data points. It is difficult to visually identify changes introduced by the initiation and propagation of cracks from the raw data (figure 12). The application of band-pass filter can be helpful to reduce the effect of measurement noise and uncertainty. Figure 14 shows the measurement data after filtering. The quality of the measurement data is significantly improved.

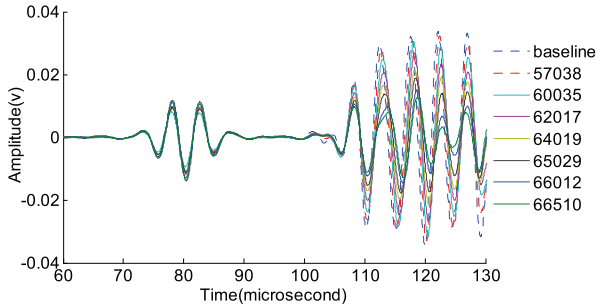

Figure 14. Filtered signal data from the sensor at different loading cycles for specimen T3.

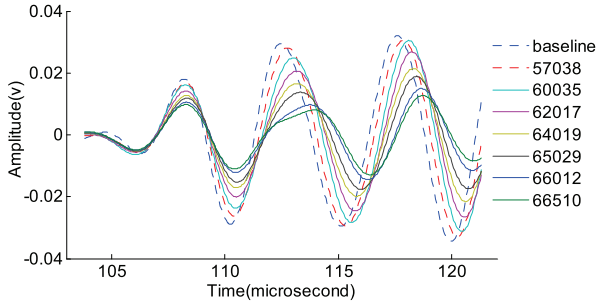

Figure 15. Filtered signal data clipped to the calculated time window (specimen T3).

As mentioned before, the desired time window is calculated based on equations (1) and (2). Figure 15 shows the first Lamb wave package arriving at the target area. In addition to the PZT data acquisition, crack length information is also recorded using microscopic imaging. A digital image processing software is employed to measure the crack length using the image registration technique from the recorded images. A representative example of observed crack through the microscope at 66 510 loading cycles is shown in figure 16.

Direct use of the measured signal for estimating crack size is difficult and data reduction is generally required to extract the damage feature. Three possible damage features from the measurement data to characterize the damage are investigated, namely, the correlation coefficient, normalized amplitude, and phase change between the damage signal and the baseline signal. Mechanisms for choosing these three features are illustrated in figure 17. The correlation coefficient depends only on signal shape changes [37]. When Lamb waves pass through a region with cracks or discontinuities, the transmitted waves are modified because of forward scattering [34, 23, 37, 38]. The signal from the actuator–sensor path that has discontinuities is affected by the presence of the damage, and the correlation coefficient between the baseline signal and the signal from the damaged specimen changes. As shown in figure 17(a), the signal from actuator–sensor paths without damage would remain intact [38]. As the damage size increases, the correlation coefficient is expected to be reduced from that of the undamaged specimen [38], and dissimilar intensities of signal changes can be an indicator of the damage area. Another feature used here is the amplitude change. The wave amplitude reflects the energy carried by the signal. Due to reflection and scattering at the crack location, the energy of the received signal reduces as the crack size increases (figure 17(b)). Thus, amplitude change can serve as a potential feature for crack size increment. An additional feature is the phase change in the signal due to the fact that the traveling distance of the wave is different for different crack sizes (figure 17(c)). The TOF of the received signal for different crack sizes increases with the crack size. Based on the mechanisms discussed above, the three features are expected to show a monotonic trend with respect to the crack size. It should be noted that complex wave propagation and boundary reflections also contaminate the received signal. Uncertainties in the local damage geometry also affect the received signal.

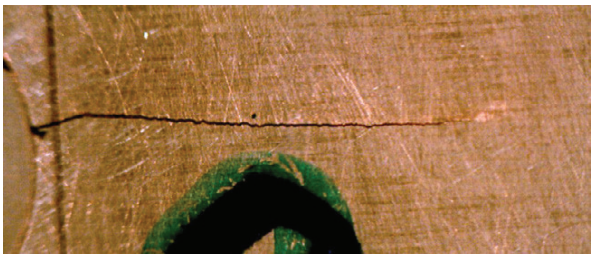

Figure 16. Crack observed from the microscope at 66 510 loading cycles (specimen T3).

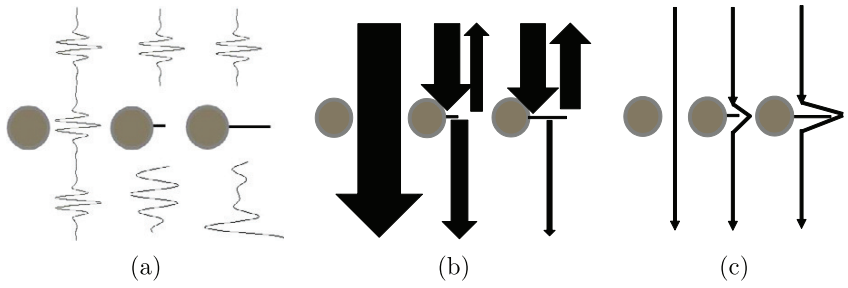

Figure 17. Illustration of changes for Lamb waves passing through a rivet hole with cracks. (a) Signal time series, (b) signal maximum amplitudes, and (c) signal phase.

Table 2. Experimental results (specimen T3) of crack size measurement, and the change in the three characteristic variables (correlation coefficient, amplitude, and phase change) introduced by the change of crack size.

Number of load cycles	Crack length (mm)	Correlation coefficient	Amplitude change (V)	Phase change (ms)
0	0	1	0.0180	0
57 038	2.57	0.9527	0.0167	0.25
60 035	4.02	0.8401	0.0161	0.5
62 017	4.72	0.7511	0.0142	0.65
64 019	5.49	0.7139	0.0127	0.7
65 029	5.90	0.6013	0.0118	0.85
66 012	6.52	0.3884	0.0105	1.05
66 510	6.93	0.3259	0.0098	1.15

The discussion on feature extraction above only serves as a general guideline for feature selection and extra care in using the three features must be taken for different applications.

Table 2 presents experimental results of the crack size versus the number of load cycles (columns 1 and 2). The measurement data labeled as zero cycle is used as the baseline signal, i.e., data for the plate without fatigue damage. Results for the three features: the correlation coefficient, the (peak) normalized amplitude, and the phase change are shown in table 2, columns 3–5. As indicated by the results, the correlation coefficient decreases as the crack length increases, the normalized amplitude also decreases with the increasing crack length, and the phase change goes up as the crack length increases. Observed trends agree with the previously discussed mechanisms for the three features, indicating that the proposed features are appropriate for crack size quantification.

4. Feature integration

The experimental procedure and signal processing technique described above are carried out for all seven specimens. The crack length versus the three features are presented in figures 18, 19 and 20. Taking specimen T1 in figure 18 as an example, cycle numbers are labeled next to the data points to show how the trend varies as the number of fatigue loading cycle increases. It is observed that the general monotonic trends are valid for all specimens under different loading conditions, which further confirms the effectiveness of the three features. It is also observed that each specimen has a unique trend that does not overlap with trends of other specimens. Due to manufacturing and loading variability, each specimen may have unique crack orientation, sensor variability, boundary conditions, and sensor installation variability. The received signal and extracted features from each of the specimens will finally encode those uncertainties. This observation clearly indicates that a single feature cannot be used to predict the crack size for other specimens due to those uncertainties. Bayesian updating can be used to reduce the uncertainties [39, 40].

It is possible that the variability or uncertainty associated with each of the specimens can be reduced by combining

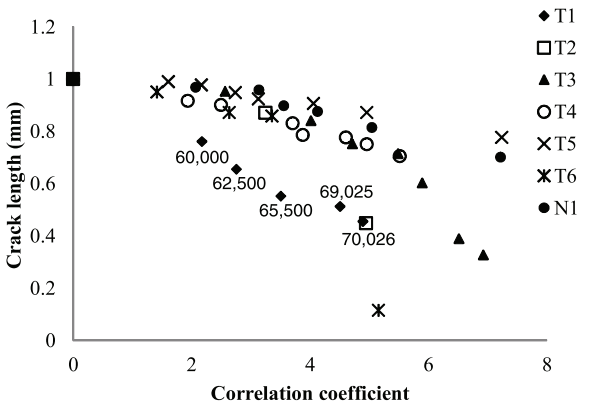

Figure 18. Crack length versus correlation coefficient for all seven riveted lap joint specimens.

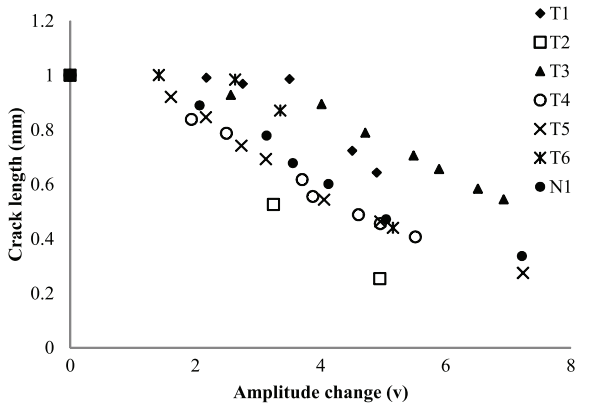

Figure 19. Crack length versus amplitude curves for all seven riveted lap joint specimens.

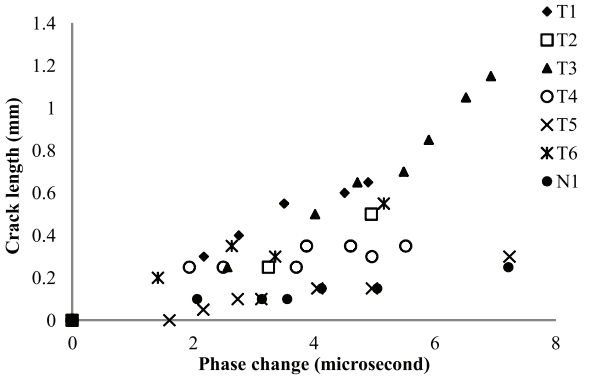

Figure 20. Crack length versus phase change curves for all seven riveted lap joint specimens.

different features together. A multi-feature integration method based on a second-order multivariate model is proposed. The model is given in equation (3).

$$a = A + \alpha_1 x + \alpha_2 y + \alpha_3 z + \alpha_4 xy + \alpha_5 xz + \alpha_6 yz + \alpha_7 x^2 + \alpha_8 y^2 + \alpha_9 z^2 \quad (3)$$

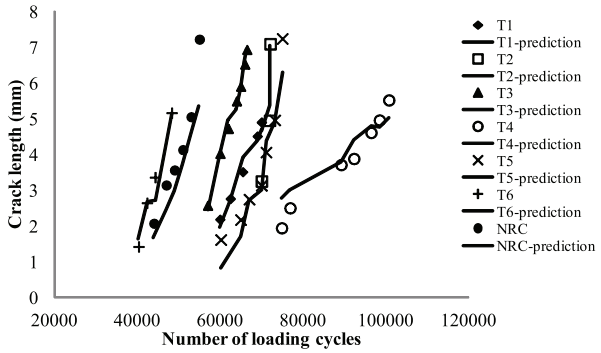

Figure 21. Experimental data (training data and validation data, discrete points) and the model predictions (solid line).

Table 3. Model parameter estimation results.

Coefficient	Value
A	7.91
α_1	−2.76
α_1	−2.67
α_1	−9.41
α_1	0.52
α_1	−5.18
α_1	10.02
α_1	6.21
α_1	0.67
α_1	3.49

where a is the crack length, x is the correlation coefficient, y is the phase change, and z is the amplitude change. Regression analysis with experimental data is made to estimate the model parameters and validate the effectiveness of the model. In this study, constant amplitude fatigue testing is performed using NASA specimens (T1, T2, T3, T5 and T6) and the results are used for model parameter estimation. Experimental data from the NRC specimen under constant loading and the specimen T4 under variable loading are used as validation data since the two exhibit uncertainties due to loading and manufacturing. The least squares method is used for model parameter estimation and the results are presented in table 3.

Figure 21 presents experimental data and model predictions. It is observed that the proposed multi-feature model agrees with the general trend for all specimens. To further validate the prediction and fitting performance, median and 95% bound predictions are shown in figure 22(a), where the x-axis is the measured crack size and the y-axis is the predicted crack size. In figure 22(a), all training data are shown as circles and validation data are shown as solid squares and triangles. It can be seen that the median prediction of the model generally characterizes the crack length and most of the data points are within the 95% prediction bounds.

To further investigate the performance improvement of using the proposed multi-feature integration predictive model, comparisons are made between the three single features and multi-feature integration. The single feature models are obtained by removing unrelated feature variables and their coefficients from equation (3). For example, the single feature model incorporating only the correlation coefficient is $a(x) = A + \alpha_1 x + \alpha_7 x^2$ (by removing terms involving y and z from equation (3)). The same training data are used to obtain model parameters using the resulting single feature model. The NRC and variable loading specimen data are still used for validations. For demonstration purposes, the standard deviation of the prediction error for the validation specimen data is used as a performance metric. A smaller value of the standard deviation of the prediction error indicates better predictive performance. Similar to figure 22(a), median 95% bound predictions are calculated. The results of the three single feature models are presented in figures 22(b)–(d) for correlation coefficient, phase change, and amplitude change, respectively. Comparing with single feature models, 95% bound predictions using the multi-feature integration model has the most compact scattering width. The fitting performance in terms of R-square and standard error is shown in the bottom-right corner of each figure. The multi-feature integration model yields the largest R-square (0.96) and the smallest standard error (0.51), indicating the best fitting performance among all models. The standard deviations of prediction error for the validation specimen data are shown in figure 23, where the multi-feature integration model yields the smallest value of 0.42. The standard deviations of the prediction error for models using single feature correlation coefficient, phase change, and amplitude change are 1.18, 1.53, 0.63, respectively.

5. Conclusions

The study presents an experimental and modeling study using Lamb waves to predict crack size in riveted lap joints. Seven specimens from different manufacturers and under different loading conditions are used to obtain measurement data using *in situ* fatigue testing and microscopic imaging techniques. Experimental data are analyzed and three damage features are proposed for coupling the crack length and the sensor measurement data. Based on the three features, a multi-feature integration method is proposed for crack size prediction using sensor measurement data. Data from five specimens are used for model parameter estimation and two specimens are used for method validation. Several conclusion are drawn based on the current study.

- Lamb wave based technique can be used to effectively quantify naturally initiated fatigue cracks in fuselage lap joints.
- Three damage features are proposed. (1) The correlation coefficient between the damage state and the healthy state, (2) the normalized amplitude between the damage state and the healthy state, and (3) the phase change between the damage state and the healthy state. The effectiveness of the three features is validated using the testing data.
- The multi-feature integration method proposed in this study can reduce the variability or uncertainty associated with different specimens and is able to predict the crack lengths for different specimens under different

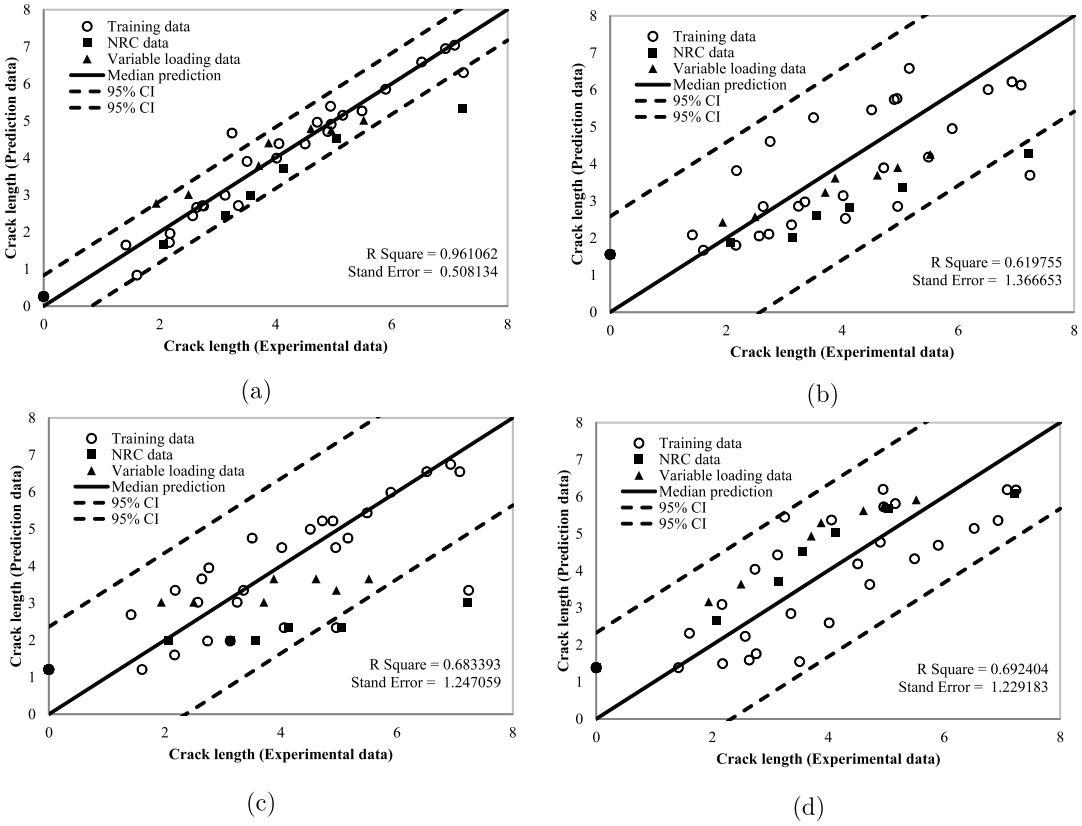

Figure 22. Median and bound predictions using the multi-feature model and single feature models. (a) Multi-feature integration, (b) single feature: correlation coefficient, (c) single feature: phase change, and (d) single feature: amplitude change.

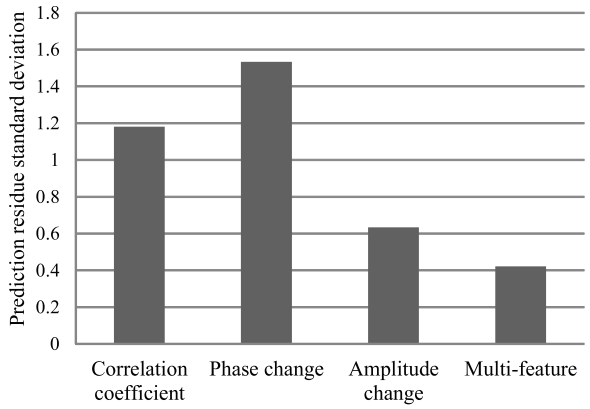

Figure 23. Comparison of model predictive performance using the multi-feature integration model and single feature models. Performance is defined as the standard deviation of the prediction error on the validation specimen data. *x*-axis represents models and *y*-axis represents the standard deviation of prediction error (a smaller value indicates a better predictive performance).

loading conditions. A second-order multivariate regression model can give satisfactory prediction performance and outperform single feature models in terms of fitting and prediction performance.

It should be noted that the current study assumes some prior knowledge of the crack location. Future work will address how to automatically detect the crack location from a sensor network. In addition, the proposed second-order multivariate regression is only meant to demonstrate the basic idea for the multi-feature integration method. Optimal selection and utilization of those features need further study. The applicability of the proposed method to other structural and material systems, such as composite skins, also needs further investigation.

Acknowledgments

The research reported in this paper was supported by the NASA ARMD/AvSP IVHM and SSAT projects under NRANNX09AY54A. The support is gratefully acknowledged. The authors also thank the in-kind support for testing specimens and technical discussions with Dr Min Liao at NRC Canada and Mr Mike Venti of NASA Dryden Flight Research Center for providing and manufacturing additional test specimen.

References

[1] Sun K, Meng G, Li F, Ye L and Lu Y 2010 Damage identification in thick steel beam based on guided ultrasonic waves *J. Intell. Mater. Syst. Struct.* **21** 225–32

[2] Kessler S S, Spearing S M and Soutis C 2002 Damage detection in composite materials using Lamb wave methods *Smart Mater. Struct.* **11** 269

[3] Kessler S S and Spearing S M 2003 Selection of materials and sensors for health monitoring of composite structures *MRS Proc.* **785** 365–75

[4] Lamb H 1917 On waves in an elastic plate *Proc. R. Soc.* A **93** 114–28

[5] Viktorov I A 1967 *Rayleigh and Lamb Waves: Physical Theory and Applications* vol 147 (New York: Plenum)

[6] Su Z and Ye L 2005 Lamb wave propagation-based damage identification for quasi-isotropic cf/ep composite laminates using artificial neural algorithm: part i-methodology and database development *J. Intell. Mater. Syst. Struct.* **16** 97–111

[7] Li F, Su Z, Ye L and Meng G 2006 A correlation filtering-based matching pursuit (cf-mp) for damage identification using Lamb waves *Smart Mater. Struct.* **15** 1585

[8] Su Z and Ye L 2005 A fast damage locating approach using digital damage fingerprints extracted from Lamb wave signals *Smart Mater. Struct.* **14** 1047

[9] Su Z, Ye L and Lu Y 2006 Guided Lamb waves for identification of damage in composite structures: a review *J. Sound Vib.* **295** 753–80

[10] Ihn J-B and Chang F-K 2004 Detection and monitoring of hidden fatigue crack growth using a built-in piezoelectric sensor/actuator network: II. Validation using riveted joints and repair patches *Smart Mater. Struct.* **13** 621

[11] Ihn J-B and Chang F-K 2004 Detection and monitoring of hidden fatigue crack growth using a built-in piezoelectric sensor/actuator network: I. Diagnostics *Smart Mater. Struct.* **13** 609

[12] Zhao X, Gao H, Zhang G, Ayhan B, Yan F, Kwan C and Rose J L 2007 Active health monitoring of an aircraft wing with embedded piezoelectric sensor/actuator network: I. Defect detection, localization and growth monitoring *Smart Mater. Struct.* **16** 1208

[13] Park G, Farrar C R, di Scalea F L and Coccia S 2006 Performance assessment and validation of piezoelectric active-sensors in structural health monitoring *Smart Mater. Struct.* **15** 1673

[14] Ihn J-B and Chang F-K 2008 Pitch–catch active sensing methods in structural health monitoring for aircraft structures *Struct. Health Monit.* **7** 5–19

[15] Raghavan A and Cesnik C E S 2007 Review of guided-wave structural health monitoring *Shock Vib. Dig.* **39** 91–116

[16] Lin X and Yuan F G 2001 Diagnostic Lamb waves in an integrated piezoelectric sensor/actuator plate: analytical and experimental studies *Smart Mater. Struct.* **10** 907

[17] Giurgiutiu V 2003 Lamb wave generation with piezoelectric wafer active sensors for structural health monitoring *Smart Struct. Mater. Proc. SPIE* **5056** 111–22

[18] Giurgiutiu V 2005 Tuned Lamb wave excitation and detection with piezoelectric wafer active sensors for structural health monitoring *J. Intell. Mater. Syst. Struct.* **16** 291

[19] Santoni G B *et al* 2007 Lamb wave-mode tuning of piezoelectric wafer active sensors for structural health monitoring *J. Vib. Acoust.* **129** 752

[20] Lemistre M and Balageas D 2001 Structural health monitoring system based on diffracted Lamb wave analysis by multiresolution processing *Smart Mater. Struct.* **10** 504

[21] Monkhouse R S C, Wilcox P D and Cawley P 1997 Flexible interdigital pvdf transducers for the generation of Lamb waves in structures *Ultrasonics* **35** 489–98

[22] Ward M D *et al* 1990 *In situ* interfacial mass detection with piezoelectric transducers *Science* **249** 1000

[23] Giurgiutiu V, Zagrai A and Bao J J 2002 Piezoelectric wafer embedded active sensors for aging aircraft structural health monitoring *Struct. Health Monit.* **1** 41–61

[24] Greve D W, Neumann J J, Nieuwenhuis J H, Oppenheim I J and Tyson N L 2005 Use of Lamb waves to monitor plates: experiments and simulations *Proc. SPIE* **5765** 281–92

[25] Lowe M J S and Diligent O 2002 Low-frequency reflection characteristics of the s Lamb wave from a rectangular notch in a plate *J. Acoust. Soc. Am.* **111** 64

[26] Feng Y, Zhou L and Li Z 2011 Damage detection for plate-like structure using matching pursuits with chirplet atom *Proc. SPIE* **7981** 798128

[27] Saravanos D A and Heyliger P R 1995 Coupled layerwise analysis of composite beams with embedded piezoelectric sensors and actuators *J. Intell. Mater. Syst. Struct.* **6** 350–63

[28] Lowe M J S, Challis R E and Chan C W 2000 The transmission of Lamb waves across adhesively bonded lap joints *J. Acoust. Soc. Am.* **107** 1333

[29] Grondel S, Delebarre C, Assaad J, Dupuis J-P and Reithler L 2002 Fatigue crack monitoring of riveted aluminium strap joints by Lamb wave analysis and acoustic emission measurement techniques *NDT & E Int.* **35** 137–46

[30] Kažys R, Mažeika L, Barauskas R, Raišutis R, Cicėnas V and Demčenko A 2006 3d analysis of interaction of Lamb waves with defects in loaded steel plates *Ultrasonics* **44** e1127–30

[31] Coelho C K, Das S, Chattopadhyay A, Papandreou-Suppappola A and Peralta P 2007 Detection of fatigue cracks and torque loss in bolted joints *14th Int. Symp. on: Smart Structures and Materials & Nondestructive Evaluation and Health Monitoring* International Society for Optics and Photonics, p 653204

[32] Lindgren E, Aldrin J C, Jata K, Scholes B and Knopp J 2007 Ultrasonic plate waves for fatigue crack detection in multi-layered metallic structures *14th Int. Symp. on: Smart Structures and Materials & Nondestructive Evaluation and Health Monitoring* International Society for Optics and Photonics, p 653207

[33] Lissenden C J, Cho H and Kim C S 2010 Fatigue crack growth monitoring of an aluminum joint structure *AIP Conf. Proc.* **1211** 1868

[34] Chang Z and Mal A 1999 Scattering of Lamb waves from a rivet hole with edge cracks *Mech. Mater.* **31** 197–204

[35] Bellinger N C, Shi G, Prost-Domasky S and Brooks C L 2007 The role of fretting fatigue experiments in improving holistic structural integrity assessments *2007 Int. Committee of Aeronautical Fatigue-ICAF 2007* (Naples: Fatigue of Aeronautical Structures as an Engineering Challenge) pp 126–46

[36] Su Z and Ye L 2009 *Identification of Damage Using Lamb Waves: From Fundamentals to Applications* vol 48 (Berlin: Springer) pp 1–14

[37] Michaels J E 2008 Detection, localization and characterization of damage in plates with an *in situ* array of spatially distributed ultrasonic sensors *Smart Mater. Struct.* **17** 035035

[38] Lu Y, Ye L, Wang D and Zhong Z 2009 Time-domain analyses and correlations of Lamb wave signals for damage detection in a composite panel of multiple stiffeners *J. Compos. Mater.* **43** 3211–30

[39] Guan X, Liu Y, Jha R, Saxena A, Celaya J and Goebel K 2011 Comparison of two probabilistic fatigue damage assessment approaches using prognostic performance metrics *Int. J. PHM Soc.* **2** 005

[40] Guan X, Jha R and Liu Y 2011 Model selection, updating, and averaging for probabilistic fatigue damage prognosis *Struct. Safety* **33** 242–9